ACS OMEGA

http://pubs.acs.org/journal/acsodf

Article

Fabrication of Trimetallic Fe−Co−Ni Electrocatalysts for Highly Efficient Oxygen Evolution Reaction

Han Young Jung,* Jong Hwan Park, Jae Chul Ro, and Su Jeong Suh*

Cite This: *ACS Omega* 2022, 7, 45636−45641

Read Online

ACCESS | Metrics & More | Article Recommendations | Supporting Information

ABSTRACT: The development of inexpensive and well-activated water-splitting catalysts is required to reduce the use of conventional fossil fuels. In this study, a trimetallic Fe−Co−Ni catalyst was fabricated using a simple ion electrodeposition method. The metal deposition was performed using cyclic voltammetry, which was more efficient than constant-voltage deposition and significantly increased the stability of the catalyst. The synthesized material presented the morphology of a nanoflower in which the nanosheets were agglomerated. The Fe−Co−Ni catalyst exhibited excellent oxygen evolution reaction (OER) properties because the charge-transfer rate was improved owing to the synergistic effect of the metals. The OER was performed in a 1 M KOH solution using a three-electrode system, and the overpotential was 302 mV at 100 mA/cm^2. In addition, the Fe−Co−Ni catalyst exhibited excellent stability in alkaline solution for more than 48 h at 200 mA/cm^2. The results show that the method for preparing Fe−Co−Ni significantly improves its catalytic activity, and the resulting material could be used as an economical and efficient catalyst in future.

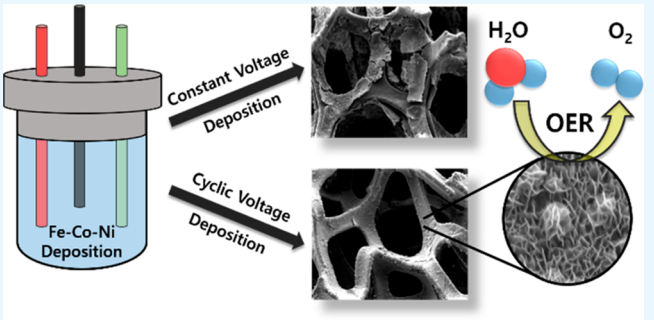

1. INTRODUCTION

Renewable hydrogen energy and electrochemical water splitting are actively being studied as alternatives to conventional fossil fuels.[1,2] Water splitting involves the hydrogen evolution reaction and oxygen evolution reaction (OER), and the half-reactions of these two electrolysis reactions are limited owing to their slow kinetics. Precious metal catalysts, which are expensive and scarce, are generally used to accelerate the slow OER.[3−5] Therefore, the development of inexpensive alternative catalyst materials with OER properties similar to those of noble metal catalysts is being actively pursued. Layered double hydroxides (LDHs) have been widely used as substitutes for OER catalyst materials.[6−10] However, LDH has limitations owing to insufficient electron-transport capacity and the shortage of exposed active sites.[11] In addition, the electrodes developed in many previous studies showed deterioration in electrode performance when a polymer binder with low electrical conductivity was used to form the catalyst layer. Therefore, research on catalyst materials that utilize the synergistic effect of the ternary metal structure to circumvent this limitation is being actively conducted.[12−15] The metal-to-metal interaction reduces the electron migration resistance, accelerates electron migration, and improves catalytic properties.[16,17]

In this study, an Fe−Co−Ni catalyst was fabricated using a simple one-step electrolytic plating method on a nickel foam substrate to improve the overall water decomposition properties. This deposition method uses a small amount of precursor and is very efficient. Moreover, economical catalyst production is possible using this strategy because precious metals are not used.[18−20] An electrode deposited using constant voltage and an electrode deposited using cyclic voltammetry (CV) under the same conditions were compared. The catalyst manufactured using the CV method had a more uniform surface than that manufactured using constant voltage, and the influence of oxygen was significantly reduced in the former. Consequently, the difference in stability between the two catalysts was large, and the catalyst manufactured using the CV method showed better characteristics. The prepared catalyst exhibited good catalytic activity, with a low overpotential (302 mV at 100 mA/cm^2) and good durability. In addition, it could be a promising economical alternative for the existing water splitting catalysts.

2. EXPERIMENTAL SECTION

2.1. Preparation of the Fe−Ni−Co on Nickel Foam Catalyst. Briefly, 0.035 mol of $FeSO_4{\cdot}7H_2O$, 0.035 mol of $CoSO_4{\cdot}7H_2O$, and 0.038 mol of $NiSO_4{\cdot}6H_2O$ were added to 200 mL of deionized water and stirred for 2 h. Ni foam (1 cm

Received: October 6, 2022
Accepted: November 18, 2022
Published: December 5, 2022

https://doi.org/10.1021/acsomega.2c06461
ACS Omega 2022, 7, 45636−45641

× 1 cm) was cleaned using water and ethanol and used as the substrate. A three-electrode system was used in the electrochemical station (CH Instruments, CHI 660E) for the deposition of the catalytic material; Ag/AgCl was used as the reference electrode, and a Pt plate (1 cm × 1 cm) was used as the counter electrode. The catalyst deposition via the constant-voltage method was performed by applying −1 V (vs reversible hydrogen electrode (RHE)) for 5 min. In the CV method, the catalyst was manufactured by performing repeated sweeping from 0 to −1 V (vs RHE). After the deposition of the catalyst material, each sample was cleaned several times with deionized water and dried at 60 °C for 2 h.

2.2. Characterization. The morphology and nanostructure of the samples were obtained using scanning electron microscopy (SEM, Philips, FEI XL 30 FEG) and transmission electron microscopy (TEM, JEOL, JEM-2100F). X-ray photoelectron spectroscopy (XPS; Vg Scienta, ESCA 2000) was performed to analyze the surfaces of the as-prepared catalysts. An inductively coupled plasma mass spectrometer (ICP-MS, PerkinElmer, NexION 2000) was used to compare the metal elements of the prepared catalyst.

2.3. Electrochemical Measurements. The electrochemical activity of the prepared electrode catalyst was evaluated using a three-electrode system with an electrochemical station (CH instrument, CHI 660E) with 1 M KOH as the electrolyte. A Hg/HgO electrode (in 1 M NaOH solution) and platinum wire were used as the reference and counter electrodes, respectively. The linear sweep voltammetry (LSV) scanning range was 0−1 V (vs Hg/HgO) at a scan rate of 5 mV/s. The kinetic properties of the catalysts were evaluated using overpotential and Tafel plots. The electrical characteristics of the sample were confirmed via electrochemical impedance spectroscopy (EIS) in the range of 0.1−100 kHz at a potential of 302 mV with an amplitude of 5 mV. All measured potentials were calibrated to the reversible hydrogen electrode (RHE) using eq 1. The pH used in the calculation was measured with a pH meter, and the value was 13.96.

$$E_{(RHE)} = E_{(Hg/HgO)} + E^{0}_{(Hg/HgO)} + (0.0591 \times pH) \quad (1)$$

3. RESULTS AND DISCUSSION

3.1. Morphological and Structural Analyses. The electrode deposited using the constant voltammetry method was referred to as Fe−Co−Ni(co) and that deposited via the CV method was referred to as Fe−Co−Ni(cv). The Fe−Co−Ni electrodes deposited using both methods showed a two-dimensional nanosheet structure similar to those of LDHs. The SEM images in Figure 1 show a comparison of the morphologies of the prepared catalysts. Many cracks were generated on the surface of Fe−Ni−Co(co) compared to that of Fe−Ni−Co(cv), showing an unstable morphology. The surface of the Fe−Ni−Co(co) microstructure was nonuniform and rough owing to the influence of gases generated during electrochemical deposition.[21] The TEM image in Figure 2 shows that the surface of the sample exhibits entangled nanosheets, and each element is evenly distributed. TEM analysis confirms the layer spacing of the fabricated Fe−Ni−Co(cv) catalysts (Figure 3). The nanostructures of the fabricated samples exhibit different interplanar distances. The crystal structure with an interplanar distance of 0.206 nm corresponds to the (111) plane of $FeNi_3$, whereas the interplanar distances of 0.27 and 0.25 nm correspond to the

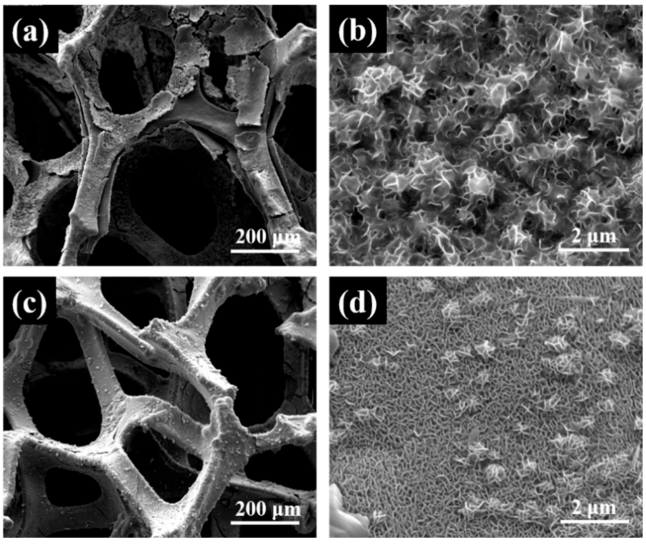

Figure 1. SEM images of Fe−Ni−Co(co) (a, b) and Fe−Ni−Co(cv) (c, d).

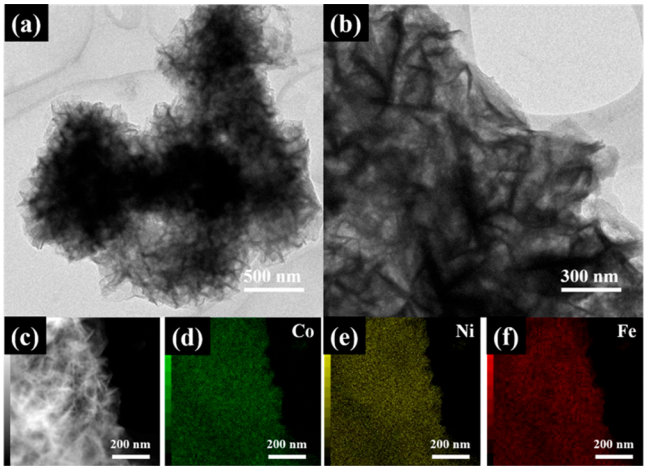

Figure 2. (a, b) TEM images of Fe−Ni−Co(cv). (c−f) Energy-dispersive X-ray spectroscopy (EDS) elemental mapping of Fe−Ni−Co(cv) sample.

(012) plane of NiFe layered double hydroxide (LDH) and FeNiCo LDH, respectively. Furthermore, the catalyst analyzed via fast Fourier-transform (FFT) analysis exhibits polycrystalline characteristics. The molar ratio of CV and CO was determined by the ICP-MS (Table S1). The molecular ratio analysis result of Fe, Ni, and Co of Fe−Ni−Co(cv) was 1.03:1.56:1, and in order to see the effect of the counter electrode on the plating process, molecular detection of Pt was attempted, but it was not detected. The binding interactions and surface oxidation states of the synthesized catalysts were analyzed using XPS. The XPS survey spectrum showed the presence of Ni, Fe, Co, and O in the sample. In Figure 4a,b, the peaks at 530.2 and 531.5 eV correspond to the metal oxide bonds and oxygen in the OH group.[22−24] For the Fe−Ni−Co(cv) sample, the peak at 533.4 eV corresponds to the oxygen-based species of surface-adsorbed H_2O.[24] The peaks at 710.6 and 725.1 eV in the Fe 2p spectrum are ascribed to the Fe^{2+} $2p_{3/2}$ and Fe^{2+} $2p_{1/2}$ states, respectively.[25] In addition, the peaks at 712.6 and 726.8 eV correspond to Fe^{3+} $2p_{3/2}$ and Fe^{3+} $2p_{1/2}$ states, respectively.[25−27] In Figure 4e,f, the peaks at 780.1

https://doi.org/10.1021/acsomega.2c06461
ACS Omega 2022, 7, 45636−45641

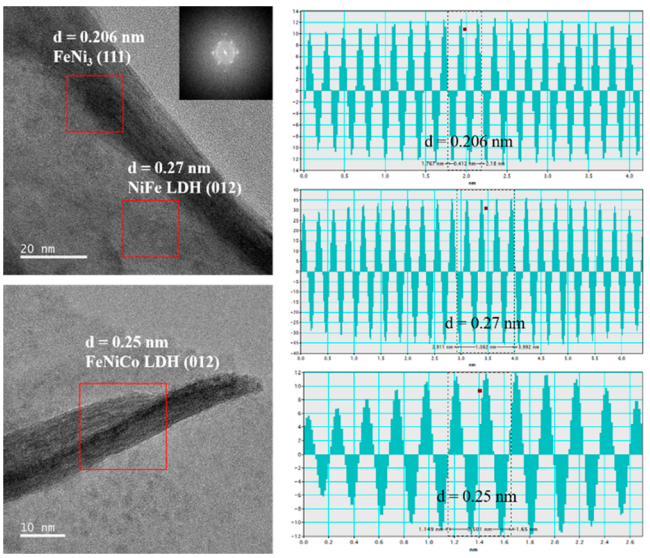

Figure 3. High-resolution transmission electron microscopy (HRTEM) images and *d*-spacing analyses of the Fe−Ni−Co(cv) catalyst.

and 795.2 eV are attributed to Co^{2+} $2p_{3/2}$ and Co^{2+} $2p_{1/2}$.[27] In the case of Fe−Ni−Co(co), the Co^{3+} $2p_{3/2}$ and Co^{3+} $2p_{1/2}$ peaks appeared at 782.5 and 797.1 eV; however, in Fe−Ni−Co(cv), they were slightly shifted owing to surface oxidation, and peaks appeared at 785.1 and 800.5 eV.[27] The peaks at 854.4 and 872.5 eV in the Ni 2p spectrum are attributed to Ni^{2+} $2p_{3/2}$ and Ni^{2+} $2p_{1/2}$. Furthermore, the peaks at 856.8 and 874.2 eV are associated with the Ni^{3+} $2p_{3/2}$ and Ni^{3+} $2p_{1/2}$ states.[27−29] The peaks at approximately 860.0 and 877.1 eV are ascribed to the satellite peaks.

3.2. OER. The Fe−Ni−Co(cv) catalyst exhibited excellent catalytic performance in reactions with alkali solutions. Figure 5a shows the LSV curve of the prepared Fe−Ni−Co(cv) catalyst; it exhibits properties superior to those of the RuO_2 catalyst. The overpotentials of the Fe−Ni−Co(cv), Fe−Ni−Co(cv), and RuO_2 catalysts measured at 100 mA/cm^2 were 302, 406, and 441 mV, respectively. Figure 5b shows a Tafel plot used to evaluate the reaction kinetics of each catalyst. The first step of the OER is the discharge step, in which the electrons adsorbed on the active site, and protons are combined to form adsorbed oxygen ions.[30−32] Thereafter, the recombination step (Tafel reaction) or desorption step (Heyrovsky reaction) occurs.[33,34] In the OER, the reaction rate is governed by the Tafel slope. Among the analyzed catalysts, the measured Tafel slope of Fe−Ni−Co(cv) was the lowest at 63 mV/dec, indicating that the catalytic reaction kinetics were the fastest. EIS analysis was performed to measure and substantiate the double-layer capacitance (C_{dl}) and charge-

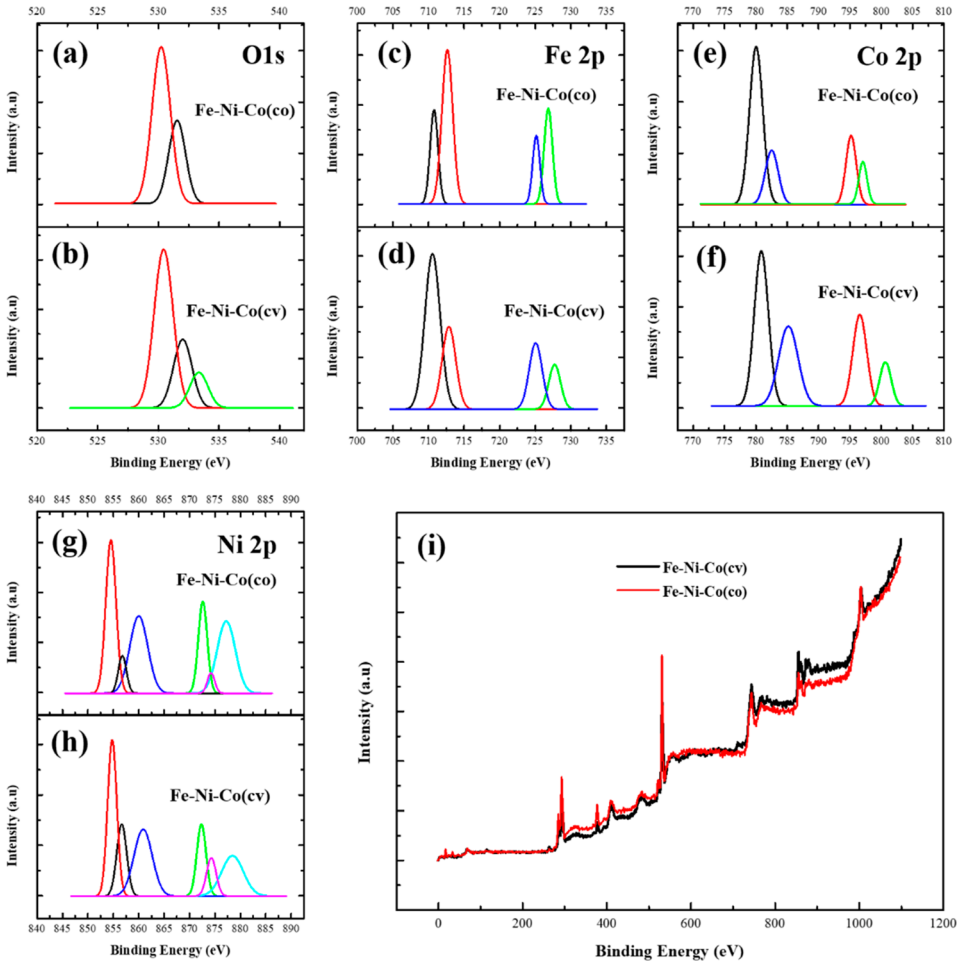

Figure 4. X-ray photoelectron spectroscopy (XPS) spectra of Fe−Ni−Co(co) and Fe−Ni−Co(cv): (a, b) O 1s peak, (c, d) Fe 2p peak, (e, f) Co 2p peak, and (g, h) Ni 2p peak, (i) survey spectrum.

https://doi.org/10.1021/acsomega.2c06461
ACS Omega 2022, 7, 45636−45641

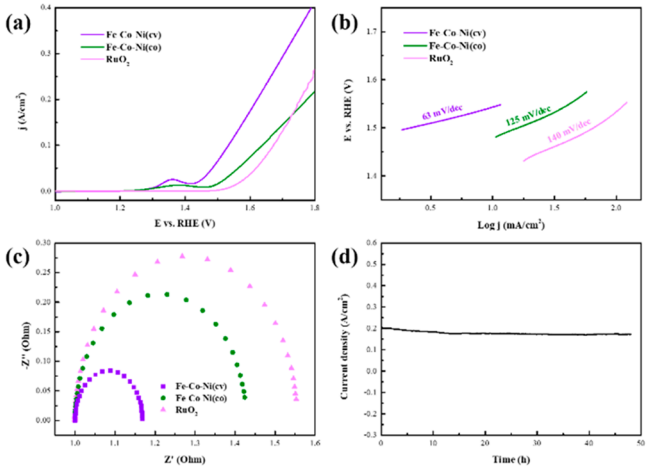

Figure 5. (a) LSV curves of Fe−Ni−Co(cv), Fe−Ni−Co(co), and commercial RuO_2 catalyst. (b) Corresponding Tafel plots. (c) Corresponding Nyquist plots. (d) Stability test for Fe−Ni−Co(cv) catalyst.

transfer resistance (R_{ct}) in the CV analysis, disproving the effective surface area of the catalyst.[35−38] The Nyquist plots of all samples are shown in Figure 5c, and the results show the lowest R_{ct} (1.42 Ω) value for Fe−Ni−Co(cv). In addition, the stability evaluation of the Fe−Ni−Co(cv) catalyst shown in Figure 5d indicates that it has excellent durability for more than 48 h at high current density (200 mA/cm^2). Figure 6a

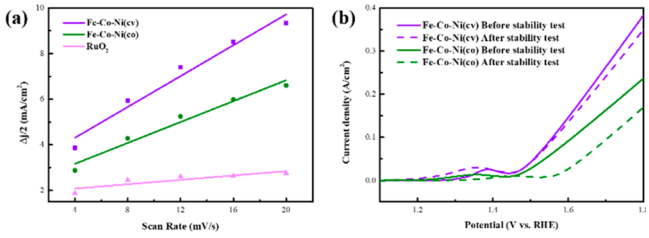

Figure 6. (a) Scan-rate dependence of the current densities of Fe−Ni−Co(cv), Fe−Ni−Co(co), and RuO_2 catalyst. (b) Comparison of OER properties before and after stability test of Fe−Ni−Co(cv) and Fe−Ni−Co(co) catalysts.

shows CV measurements for all samples at different scan rates (4, 8, 12, 16, and 20 mV/s) in the 0.1−0.2 V vs RHE scale region. The electrochemical surface area (ECSA) can be calculated using eq 2, and it is directly proportional to C_{dl} because C_s represents a constant theoretical value of the material.[39−42]

$$\text{ECSA} = C_{dl}/C_s \quad (2)$$

Fe−Ni−Co(cv) has a C_{dl} value of 33.78 mF/cm^2, which is higher than those of Fe−Ni−Co(co) (22.87 mF/cm^2) and RuO_2 (4.78 mF/cm^2), indicating the highest catalytic activity (Figure S4). As a result of ECSA analysis, it was confirmed that the surface area and active site exposure of the Fe−Ni−Co(cv) sample were higher than that of the RuO_2 and Fe−Ni−Co(co) samples. Figure 6b shows a comparison of the LSV curves before and after the stability test. In the case of Fe−Ni−Co(cv), the overpotential before and after the test showed a minimal difference of less than 0.5%, whereas in the case of Fe−Ni−Co(co), a loss of more than 6% occurred. The results show that the amount of gas generated on the surface during the deposition process of the Fe−Ni−Co(cv) sample was reduced, preventing oxygen from entering the metal and improving the adhesion. The OER characteristics of the prepared catalyst were compared with other reported transition-metal-based catalysts, and the results was listed in Table 1.

Table 1. Summary of Research on Ni-, Fe-, and Co-Based Catalysts in Recent Years

Material	Overpotential at 10 mA/cm^2 (mV)	Overpotential at 100 mA/cm^2 (mV)	Tafel slope (mV/dec)	Ref
Co Ni	280	331	79	1
Fe−Co−Ni	280	409	86	3
Fe−Co−B	228		65	7
NiCoFe−LDH	276	332	56	8
FeCoNi alloy	285		42	10
NiFeW	249		79	12
NiFeOOH		320	60	18
NiFeCo@CNS	213	350	62	19
NiCoFe nanosheet		333	56	20
Fe−Ni−Co(cv)	~207	302	6	this work

4. CONCLUSIONS

In this study, Fe−Co−Ni catalyst was fabricated using a simple electrochemical deposition method. The catalysts prepared via constant-voltage deposition and CV deposition were compared. The CV deposition method was advantageous for achieving a uniform deposition because it reduced the amount of gas generated on the surface compared to constant-voltage deposition. In addition, because the use of the CV method prevented oxygen from penetrating the metal, the two catalysts showed a large difference in stability. The structure of the prepared sample provided a large amount of hydroxide, which acted as an intermediate for the OER and significantly reduced the overpotential. In addition, compared to single metal or bimetallic catalysts, the trimetallic catalyst has a discontinuous lattice and has an advantageous structure for OER due to increased exposure of surface defects due to the cation-exchange process. The measured overpotential of the catalyst was 302 mV at 100 mA/cm^2, which indicated better catalytic properties than those of RuO_2. The excellent OER performance in this paper is attributed to the structure with a large surface area of Fe−Ni−Co and the exposure of many active sites. In addition, it exhibits easy electron transport kinetics due to the synergistic effect between metal elements. This study demonstrates a method for preparing a catalyst with a high catalytic activity using a low-cost metal, which could be used in oxygen-based energy-conversion technologies.

■ ASSOCIATED CONTENT

Supporting Information

The Supporting Information is available free of charge at https://pubs.acs.org/doi/10.1021/acsomega.2c06461.

SEM image according to applied voltage in manufacturing Fe−Ni−Co(co) catalyst, SEM image according to the number of repetitions in manufacturing Fe−Ni−

https://doi.org/10.1021/acsomega.2c06461
ACS Omega 2022, 7, 45636−45641

Co(cv) catalyst, LSV curves for each condition, cyclic voltammograms for each catalyst, HER characterization of Fe−Ni−Co(cv) samples, ICP-MS analysis results (PDF)

AUTHOR INFORMATION

Corresponding Authors

Han Young Jung − *Sungkyunkwan University (SKKU), Suwon-si, Gyeonggi-do 16419, Republic of Korea;* orcid.org/0000-0002-4038-0840; Email: boomwin3@skku.edu

Su Jeong Suh − *Sungkyunkwan University (SKKU), Suwon-si, Gyeonggi-do 16419, Republic of Korea;* orcid.org/0000-0002-4950-8601; Email: suhsj@skku.edu

Authors

Jong Hwan Park − *Sungkyunkwan University (SKKU), Suwon-si, Gyeonggi-do 16419, Republic of Korea*

Jae Chul Ro − *Sungkyunkwan University (SKKU), Suwon-si, Gyeonggi-do 16419, Republic of Korea*

Complete contact information is available at: https://pubs.acs.org/10.1021/acsomega.2c06461

Notes

The authors declare no competing financial interest.

ACKNOWLEDGMENTS

This work was supported by the Gyeonggi Regional Research Center (GRRC) program of Gyeonggi Province (GRRC Sungkyunkwan 2017-B01) and the Korea Basic Science Institute (KBSI) National Research Facilities & Equipment Center (NFEC) grant funded by the Korean government (Ministry of Education) (2019R1A6C1010031).

REFERENCES

(1) Charles, V.; Zhang, X.; Yuan, M.; Zhang, K.; Cui, K.; Zhang, J.; Zhao, T.; Li, Y.; Liu, Z.; Li, B.; Zhang, G. CoNi nano-alloy anchored on biomass-derived N-doped carbon frameworks for enhanced oxygen reduction and evolution reactions. *Electrochim. Acta* **2022**, *402*, 402.

(2) Chae, M.; Jung, H. y.; Suh, S. J. Fabrication of platinum-doped WS_2 hollow spheres catalyst for high-efficient hydrogen evolution reaction. *J. Appl. Electrochem.* **2022**, *52* (3), 499−507.

(3) Zhu, S.; Lei, J.; Wu, S.; Liu, L.; Chen, T.; Yuan, Y.; Ding, C. Construction of Fe-Co-Ni-S_x/NF nanomaterial as bifunctional electrocatalysts for water splitting. *Mater. Lett.* **2022**, *311*, 131549.

(4) Gu, X.; Zheng, S.; Huang, X.; Yuan, H.; Li, J.; Kundu, M.; Wang, X. Hybrid Ni_3S_2-MoS_2 nanowire arrays as a pH-universal catalyst for accelerating the hydrogen evolution reaction. *Chem. Commun.* **2020**, *56* (16), 2471−2474.

(5) Tian, X.; Li, X.; Duan, S.; Du, Y.; Liu, T.; Fang, Y.; Yang, X. Room Temperature Benzofused Lactam Synthesis Enabled by Cobalt (III)-Catalyzed C (sp2)−H Amidation. *Advanced Synthesis and Catalysis* **2021**, *363* (4), 1050−1058.

(6) Liu, J.; Choi, H. J.; Meng, L. Y. A review of approaches for the design of high-performance metal/graphene electrocatalysts for fuel cell applications. *Journal of Industrial and Engineering Chemistry*; Korean Society of Industrial Engineering Chemistry, 2018; Vol. *64*, pp 1−15.

(7) Yang, P.; Li, E.; Xiao, F.; Zhou, P.; Wang, Y.; Tang, W.; He, P.; Jia, B. Nanostructure Fe−Co−B/bacterial cellulose based carbon nanofibers: An extremely efficient electrocatalyst toward oxygen evolution reaction. *Int. J. Hydrogen Energy* **2022**, *47* (26), 12953−12963.

(8) Wang, Y.; Tao, S.; Lin, H.; Wang, G.; Zhao, K.; Cai, R.; Yang, S. Atomically targeting NiFe LDH to create multivacancies for OER catalysis with a small organic anchor. *Nano Energy* **2021**, *81*, 105606.

(9) Chen, J.; Zheng, F.; Zhang, S. J.; Fisher, A.; Zhou, Y.; Wang, Z.; Sun, S. G. Interfacial Interaction between FeOOH and Ni-Fe LDH to Modulate the Local Electronic Structure for Enhanced OER Electrocatalysis. *ACS Catal.* **2018**, *8* (12), 11342−11351.

(10) Zhang, X.; Zhao, Y.; Zhao, Y.; Shi, R.; Waterhouse, G. I. N.; Zhang, T. A Simple Synthetic Strategy toward Defect-Rich Porous Monolayer NiFe-Layered Double Hydroxide Nanosheets for Efficient Electrocatalytic Water Oxidation. *Adv. Energy Mater.* **2019**, *9* (24), 1900881.

(11) Guo, R.; Wen, H.; Zhang, S.; Yu, T.; He, Y.; Ni, Z.; You, J. Anionic sulfur-modified FeNi-LDH at various Fe/Ni molar ratios for high-performance OER electrocatalysis. *Mater. Lett.* **2021**, *285*, 285.

(12) Qin, Y.; Wang, F.; Shang, J.; Iqbal, M.; Han, A.; Sun, X.; Xu, H.; Liu, J. Ternary NiCoFe-layered double hydroxide hollow polyhedrons as highly efficient electrocatalysts for oxygen evolution reaction. *Journal of Energy Chemistry* **2020**, *43*, 104−107.

(13) Zhang, L.; Lu, P.; Luo, Y.; Zheng, J. Y.; Ma, W.; Ding, L. X.; Wang, H. Graphene-quantum-dot-composited platinum nanotube arrays as a dual efficient electrocatalyst for the oxygen reduction reaction and methanol electro-oxidation. *Journal of Materials Chemistry A* **2021**, *9* (15), 9609−9615.

(14) Stevens, M. B.; Enman, L. J.; Korkus, E. H.; Zaffran, J.; Trang, C. D. M.; Asbury, J.; Kast, M. G.; Toroker, M. C.; Boettcher, S. W. Ternary Ni-Co-Fe oxyhydroxide oxygen evolution catalysts: Intrinsic activity trends, electrical conductivity, and electronic band structure. Nano. *Research* **2019**, *12* (9), 2288−2295.

(15) Xia, J.; Huang, K.; Yao, Z.; Zhang, B.; Li, S.; Chen, Z.; Wu, F.; Wu, J.; Huang, Y. Ternary duplex FeCoNi alloy prepared by cathode plasma electrolytic deposition as a high-efficient electrocatalyst for oxygen evolution reaction. *J. Alloys Compd.* **2022**, *891*, 161934.

(16) Peng, L.; Yang, N.; Yang, Y.; Wang, Q.; Xie, X.; Sun-Waterhouse, D.; Waterhouse, G. I. N. Atomic Cation-Vacancy Engineering of NiFe-Layered Double Hydroxides for Improved Activity and Stability towards the Oxygen Evolution Reaction. *Angewandte Chemie - International Edition* **2021**, *60* (46), 24612−24619.

(17) Park, H. K.; Ahn, H.; Lee, T. H.; Lee, J. Y.; Lee, M. G.; Lee, S. A.; Jang, H. W. Grain Boundaries Boost Oxygen Evolution Reaction in NiFe Electrocatalysts. *Small Methods* **2021**, *5* (2), 2170003.

(18) Liu, Y.; Song, Z.; Li, Z.; Han, M.; Cheng, Y.; Zheng, Z. Standing NiFe LDH nanosheets on stainless steel fibers felt: A synergistic impact on the oxygen evolution reaction (OER) for the water splitting. *Catal. Commun.* **2022**, *164*, 164.

(19) Guo, P. F.; Yang, Y.; Wang, W. J.; Zhu, B.; Wang, W. T.; Wang, Z. Y.; Wang, J. L.; Wang, K.; He, Z. H.; Liu, Z. T. Stable and active NiFeW layered double hydroxide for enhanced electrocatalytic oxygen evolution reaction. *Chemical Engineering Journal* **2021**, *426*, 130768.

(20) Lyu, F.; Wang, Q.; Choi, S. M.; Yin, Y. Noble-Metal-Free Electrocatalysts for Oxygen Evolution. *Small*;Wiley-VCH Verlag, 2019; Vol. *15*, Issue 1.

(21) Qi, J.; Zhang, W.; Cao, R. Solar-to-Hydrogen Energy Conversion Based on Water Splitting. *Advanced Energy Materials*; Wiley-VCH Verlag, 2018; Vol. *8*, Issue 5.

(22) Wang, X.; Liu, H.; Li, M.; Li, J.; Lu, Y.; Wang, L.; Wang, Z.; Zhang, X.; Ding, X. Modulation of electronic structure and oxygen vacancies of perovskites $SrCoO_{3-\delta}$ by sulfur doping enables highly active and stable oxygen evolution reaction. *Electrochim. Acta* **2021**, *390*, 138872.

(23) Zhang, Y.; Kizilkaya, O.; Bilan, H. K.; Kurtz, R.; Podlaha, E. J. Activity and Regeneration of Electrodeposited Fe-Ni-Co-Based Electrocatalysts for the Alkaline Oxygen Evolution Reaction. *ACS Applied Energy Materials* **2020**, *3* (8), 7239−7245.

(24) Chen, C.; Tuo, Y.; Lu, Q.; Lu, H.; Zhang, S.; Zhou, Y.; Zhang, J.; Liu, Z.; Kang, Z.; Feng, X.; Chen, D. Hierarchical trimetallic Co-Ni-Fe oxides derived from core-shell structured metal-organic

frameworks for highly efficient oxygen evolution reaction. *Applied Catalysis B: Environmental* **2021**, *287*, 119953.
(25) Kathale, B. M.; Xiao, H.; Yang, S.; Yin, H.; Yu, T.; Zhou, X.; Qian, L.; Xiao, J.; Lei, P.; Li, X. Fluoride mediated conversion of FeOOH into NiFeOOH for outstanding oxygen evolution reaction. *Electrochim. Acta* **2022**, *406*, 406.
(26) Yaseen, W.; Ullah, N.; Xie, M.; Yusuf, B. A.; Xu, Y.; Tong, C.; Xie, J. Ni-Fe-Co based mixed metal/metal-oxides nanoparticles encapsulated in ultrathin carbon nanosheets: A bifunctional electrocatalyst for overall water splitting. *Surfaces and Interfaces* **2021**, *26*, 26.
(27) Hu, H.-S.; Li, Y.; Deng, G.; Shao, Y.-R.; Li, K.-X.; Wang, C.-B.; Feng, Y.-Y. The importance of the iron valence state in NiCoFe nanosheet array catalysts for the oxygen evolution reaction. *Inorganic Chemistry Frontiers* **2021**, *8* (3), 766−776.
(28) Chandrasekaran, P.; Nesakumar Jebakumar Immanuel Edison, T.; Gopalakrishnan Sethuraman, M. Electrocatalytic study of carbon dots/Nickel iron layered double hydroxide composite for oxygen evolution reaction in alkaline medium. *Fuel* **2022**, *320*, 123947.
(29) Wang, Y.; Zhu, R.; Wang, Z.; Huang, Y.; Li, Z. Cu induced formation of dendritic CoFeCu ternary alloys on Ni foam for efficient oxygen evolution reaction. *J. Alloys Compd.* **2021**, *880*, 160523.
(30) Zhou, H.; Zhang, H.; Lai, C.; Wang, H.; Hu, J.; Ji, S.; Lei, L. Rapidly electrodeposited $NiFe(OH)_x$ as the catalyst for oxygen evolution reaction. *Inorg. Chem. Commun.* **2022**, *139*, 109350.
(31) Huang, F.; Yao, B.; Huang, Y.; Dong, Z. L. NiFe layered double hydroxide nanosheet arrays for efficient oxygen evolution reaction in alkaline media. *Int. J. Hydrogen Energy* **2022**, *47* (51), 21725−21735.
(32) Kim, C.; Kim, S. H.; Lee, S.; Kwon, I.; Kim, S.; Seok, C.; Park, Y. S.; Kim, Y. Boosting overall water splitting by incorporating sulfur into NiFe (oxy) hydroxide. *Journal of Energy Chemistry* **2022**, *64*, 364−371.
(33) Wang, S.; Xu, B.; Huo, W.; Feng, H.; Zhou, X.; Fang, F.; Xie, Z.; Shang, J. K.; Jiang, J. Efficient FeCoNiCuPd thin-film electrocatalyst for alkaline oxygen and hydrogen evolution reactions. *Applied Catalysis B: Environmental* **2022**, *313*, 121472.
(34) Wei, Y.; Lv, Y.; Guo, B.; Gong, J. Hierarchical molybdenum disulfide nanosheet arrays stemmed from nickel-cobalt layered double hydroxide/carbon cloth for highly-efficient hydrogen evolution reaction. *Journal of Energy Chemistry* **2021**, *57*, 587−592.
(35) Jung, S. Y.; Kang, S.; Kim, K. M.; Mhin, S.; Kim, J. C.; Kim, S. J.; Enkhtuvshin, E.; Choi, S.; Han, H. S. Sulfur-incorporated nickel-iron layered double hydroxides for effective oxygen evolution reaction in seawater. *Appl. Surf. Sci.* **2021**, *568*, 150965.
(36) Zhang, W.; Li, D.; Zhang, L.; She, X.; Yang, D. NiFe-based nanostructures on nickel foam as highly efficiently electrocatalysts for oxygen and hydrogen evolution reactions. *Journal of Energy Chemistry*; Elsevier B.V, 2019; Vol. *39*, pp 39−53.
(37) Rong, M.; Mo, Y.; Cao, Z.; Ma, X.; Wang, S.; Zhong, H. $MoSe_2$ regulates Ce-doped NiFe layered double hydroxide for efficient oxygen evolution reaction: The increase of active sites. *Int. J. Hydrogen Energy* **2022**, *47* (43), 18688−18699.
(38) Gu, X.; Liu, Z.; Li, M.; Tian, J.; Feng, L. Surface structure regulation and evaluation of FeNi-based nanoparticles for oxygen evolution reaction. *Applied Catalysis B: Environmental* **2021**, *297*, 120462.
(39) Gebreslase, G. A.; Martínez-Huerta, M. V.; Lázaro, M. J. Recent progress on bimetallic NiCo and CoFe based electrocatalysts for alkaline oxygen evolution reaction: A review. *Journal of Energy Chemistry*; Elsevier B.V, 2022; Vol. *67*, pp 101−137.
(40) Cao, X.; Wang, T.; Jiao, L. Transition-Metal (Fe, Co, and Ni)-Based Nanofiber Electrocatalysts for Water Splitting. Advanced Fiber. *Materials* **2021**, *3* (4), 210−228.
(41) Yang, J.; Xuan, H.; Yang, J.; Meng, L.; Wang, J.; Liang, X.; Li, Y.; Han, P. Metal-organic framework-derived FeS_2/$CoNiSe_2$ heterostructure nanosheets for highly-efficient oxygen evolution reaction. *Appl. Surf. Sci.* **2022**, *578*, 152016.
(42) Wang, L.; Zhang, L.; Ma, W.; Wan, H.; Zhang, X.; Zhang, X.; Zhou, Z. In Situ Anchoring Massive Isolated Pt Atoms at Cationic Vacancies of α-NixFe1-x$(OH)_2$ to Regulate the Electronic Structure for Overall Water Splitting. *Adv. Funct. Mater.* **2022**, *32*, 2203342.

https://doi.org/10.1021/acsomega.2c06461
ACS Omega 2022, 7, 45636−45641